Biogeosciences, 23, 4271–4286, 2026
https://doi.org/10.5194/bg-23-4271-2026

Biogeosciences Open Access EGU

Air–Sea Interactions and Biogeochemical Responses to Medicane Daniel

Babita Jangir and Ehud Strobach

Institute of Soil, Water and Environmental Sciences, Volcani Institute, Agriculture Research Organization, Rishon LeTsiyon, Israel

Correspondence: Babita Jangir (bj11@iitbbs.ac.in)

Received: 19 December 2025 – Discussion started: 2 February 2026
Revised: 14 May 2026 – Accepted: 1 June 2026 – Published: 29 June 2026

Abstract. Medicane Daniel, formed on 4–12 September 2023, stands out as the deadliest recorded storm in Mediterranean history. In this study, we investigate the role of sea features in the intensification of the medicane Daniel and the response of biogeochemical properties to the storm. Our results show that medicane Daniel intensified immediately prior to landfall in a coastal environment characterized by the co-occurrence of a warm-core eddy (WCE), elevated ocean heat content, and a moderate marine heatwave (MHW), suggesting that sea anomalies may have supported or modulated the intensification under favorable atmospheric forcing. Additionally, observations from the high-resolution Surface Water and Ocean Topography (SWOT) satellite reveal a larger anticyclonic eddy than that depicted in lower-resolution products, thereby further supporting the hypothesis of sea-induced intensification. The favorable conditions at the sea before landfall were accompanied by moisture convergence and moisture supply in the atmosphere above, leading to intense precipitation in this region. Biogeochemical properties were strongly affected by cyclone-induced subsurface vertical mixing and upwelling. Focusing on two eddies in the vicinity of the maximum cyclone intensity, we found that the observed vertical displacement of the deep chlorophyll maximum exceeds that expected by direct wind-driven upwelling alone, suggesting additional contribution from a structural isopycnal adjustment triggered by the neutralization of eddy vorticity. We propose that the medicane destabilizes the eddies' internal balance, leading to a large-scale reorganization of the water column that persists longer in the WCE than the transient response observed in the cold-core eddy (CCE).

Key points.

- Co-occurring warm-core eddies, marine heatwave, and elevated ocean heat content provided support for the rapid intensification of medicane Daniel near landfall.
- High-resolution SWOT observations indicate stronger and larger eddy structures than conventional datasets, supporting their critical role in air–sea interactions.
- Interaction with warm-core eddies amplifies vertical mixing and nutrient supply, leading to enhanced chlorophyll and productivity responses.
- Cyclone-induced biogeochemical response is influenced by subsurface restructuring and isopycnal adjustment, exceeding expectations from Ekman-driven upwelling alone.
- Results demonstrate that compound ocean extremes can significantly enhance both cyclone intensity and ocean biogeochemical impacts.

1 Introduction

The Mediterranean region is recognized as a climate change hotspot (IPCC, 2021), warming at a rate up to 1.5 times faster than the global average (MedECC, 2020; Zittis et al., 2022; Khodayar et al., 2025). Situated between the arid climate of North Africa and the temperate and wet climate of Central Europe, the Mediterranean region is particularly vulnerable to future climate impacts. Surface temperature in this region is projected to continue increasing, but the precipitation tends to decrease (Cherif et al., 2020; Reale et al., 2022). As a consequence, the magnitude of extreme events such as Mediterranean cyclones, marine heatwaves (MHWs), and intense droughts is projected to increase under future climate

scenarios (MedECC, 2020; Hochman et al., 2021; Zittis et al., 2022).

Medicanes are a subcategory of Mediterranean cyclones, which can resemble hurricanes in both intensity and impact. They often bring torrential rainfall, flash floods, powerful winds, storm surges, and hazardous sea conditions. Such events pose significant risks, particularly to coastal communities and urban centers, threatening homes, livelihoods, and natural ecosystems (Hochman et al., 2021; Khodayar et al., 2025). Similar to Mediterranean cyclones, medicane's intensity is projected to increase under future climate scenarios, but with lower frequency (González-Alemán et al., 2019). Despite their strong impact, the full extent of the damage medicanes inflict, both socially and economically, remains insufficiently understood. Moreover, their potential impact on ocean biogeochemistry is under-researched and often poorly communicated, leaving a critical gap in public awareness and scientific insight.

Medicanes are also known as "tropical-like cyclones" because they have tropical cyclone-like characteristics such as a cloud-free calm "eye", spiralling cloud bands, and strong winds near the vortex centre. These features may be associated with the absence of fronts, weak vertical wind shear, and a warm-core with an axisymmetric structure (Miglietta and Rotunno, 2019; Flaounas et al., 2022; Panegrossi et al., 2023). The formation of cyclones in the Mediterranean region including medicanes, is primarily driven by baroclinic instability and Rossby wave breaking (Raveh-Rubin and Flaounas, 2017; Flaounas et al., 2022). As these systems evolve and reach their mature stage, medicanes can intensify and be sustained through exchanges of heat and momentum at the air-sea interface (Emanuel, 2005). The development of intense Mediterranean cyclones is frequently associated with southward shifts of the polar jet, which enable air masses with high potential vorticity to enter the Mediterranean region, thereby initiating baroclinic instability similar to that observed during extratropical cyclone development over open oceans (Flocas, 2000; Trigo et al., 2002; Nicolaides et al., 2006; Fita et al., 2007; Claud et al., 2010; Kouroutzoglou et al., 2011; Flaounas et al., 2015). Raveh-Rubin and Flaounas (2017) identified Rossby wave breaking as a frequent precursor to Mediterranean cyclogenesis, while Flaounas et al. (2015) further emphasized that the cyclogenesis environment in the region is characterized by strong horizontal shear, driving these cyclones to follow a typical baroclinic life cycle. Furthermore, Flaounas et al. (2025) also highlight the importance of these atmospheric variables in the genesis and intensification of medicane Daniel. In this manuscript, we primarily focus on potential atmospheric and oceanic precursors that are associated with Daniel's intensification and ensuing precipitation.

Furthermore, the role of underlying ocean eddies and MHWs in modulating the deepening of a cyclone is often overlooked. Recent studies have highlighted the critical role of ocean eddies and MHWs in modulating cyclone's deepening in the Mediterranean region (Jangir et al., 2023, 2024; Mishra et al., 2024; Strobach et al., 2024). In particular, Jangir et al. (2024) demonstrated the significant intensification of medicane Ianos due to the presence of a strong MHW, making it the only category 2 cyclone observed in the Mediterranean Sea. In contrast, other medicanes such as Zorbas and Apollo intensified primarily due to the interaction with warm-core eddies (WCEs) along their paths. Mishra et al. (2024) reported that if we remove these Sea Surface Temperature (SST) anomalies from the path of medicane Ianos, the medicane will still form, but with a reduced intensity. Strobach et al. (2024) reported that ocean mesoscale eddies in the Eastern Mediterranean can significantly influence extreme weather, as shown during the heavy rainfall event in Israel that occurred from 8 to 10 January 2020. High-resolution coupled ocean-atmosphere simulations captured the event more accurately than uncoupled ones. The study by Strobach et al. (2024) highlights how eddies can enhance atmospheric moisture and meso-cyclone development, intensifying local extremes.

As efforts continue to enhance the accuracy of cyclone intensity forecasts, the potential influence of eddies, MHWs, and ocean heat content (OHC) remains a critical yet less explored aspect, particularly within the Mediterranean context. To improve the prediction of Mediterranean cyclones and mitigate associated risks, a deeper understanding of air-sea interaction processes, specifically surface heat fluxes, momentum fluxes, and upper-ocean thermodynamic responses, and the role of pre-existing oceanic conditions in cyclone genesis and intensification, is essential. Recent studies have increasingly focused on these dynamics, exploring how air-sea exchanges affect not only medicanes intensity but also the ocean's biogeochemical responses (Jangir et al., 2023; Menna et al., 2023; Scardino et al., 2024; Avolio et al., 2024). Notably, Jangir et al. (2023) highlighted the influence of WCEs on the intensification of medicanes, demonstrating that eddy size also plays a critical role; larger eddies tend to promote stronger cyclones and heavier rainfall. In this particular study, we show the influence of eddies and MHW on the intensity of medicane Daniel.

Most of the studies use the satellite sea level anomaly (SLA) altimetry data from the Copernicus Marine Services (CMEMS) for the detection of eddies. Here, we also use the Surface Water and Ocean Topography (SWOT) satellite data, which are available at high spatial resolution. The SWOT satellite provides the first-ever global observations of ocean dynamics at sub-mesoscale spatial resolutions (1–100 km). While traditional satellite products, such as those from the Copernicus mission, offer spatial resolutions of approximately 25 km globally and 12.5 km in the Mediterranean Sea, SWOT's advanced wide-swath altimetry overcomes these limitations by achieving resolutions as fine as 250 m to 2 km. This enhanced capability enables the detection of small-scale ocean features that were previously misrepresented. SWOT observations confirm the widespread

presence of sub-mesoscale eddies and internal waves, particularly energetic in regions like western boundary currents and the Antarctic Circumpolar Current (Archer et al., 2025; Tranchant et al., 2025). This high-resolution data is especially valuable for studying ocean-atmosphere interactions, such as the role of eddies in cyclone intensification. In particular, SWOT's ability to capture the structure, intensity, and evolution of eddies provides critical insight into how these features influence heat transport, vertical mixing, and the modulation of cyclone intensity due to eddies. Thus, SWOT marks a transformative step in advancing our understanding of fine-scale ocean processes and their implications for weather, climate, and marine biogeochemistry.

Atmospheric cyclones are known to trigger substantial phytoplankton blooms (Shang et al., 2015; Chowdhury et al., 2020; Liu et al., 2020). These blooms are primarily attributed to cyclone-induced upwelling and vertical mixing, which transport cold, nutrient-rich, or chlorophyll-loaded water into the euphotic zone, stimulating phytoplankton bloom. Such storm-driven biological responses offer valuable insight into ocean mixing and biogeochemical dynamics (Chen et al., 2022). Additionally, strong cyclonic winds often cause a noticeable decrease in SST, which plays a crucial role in regulating primary productivity (Latha et al., 2015). There are a few studies reported in the other ocean basins that indicate the enhancement of chlorophyll *a* (Chl *a*) concentration following the passage of a cyclone in the presence of eddies (Dutta et al., 2019; Zhang and Qiu, 2020; Vidya et al., 2021) and MHW (Oliver et al., 2018; Jangir et al., 2024). Recently, a study by Scardino et al. (2025) reported the response of Mediterranean cyclones on ocean chlorophyll concentration, primarily using Bio-Argo floats. In contrast, our study offers a new perspective by utilizing subsurface profiles of a broader suite of biogeochemical variables, including chlorophyll, phytoplankton, nutrients, and oxygen concentration, complemented by multiple ocean satellite and reanalysis products. To date, such a comprehensive assessment has rarely been reported for the Mediterranean Sea. Here, we investigate the impact of medicane Daniel on ocean biogeochemistry in the context of the SST anomalies along its path.

In this study, we highlight the co-occurrence of compound extreme events in the region prior to medicane Daniel's landfall. Specifically, we show that the intensification of medicane Daniel may have been driven by the combined influence of a WCE and an MHW. We examine the key atmospheric and oceanic factors that contributed to Daniel's development. The analysis also highlights the unique perspective offered by the SWOT satellite, capturing aspects of air-sea interaction that traditional datasets do not resolve. Additionally, we investigate the medicane's impact on ocean biogeochemistry along its path, and specifically at the WCE location prior to landfall, providing insights into the underlying physical and biological processes that govern such interactions.

2 Synoptic evolution and impacts of medicane Daniel

On 2–3 September, a swift cold front traversed Central Europe, generating an upper-level trough that created a cut-off low near Greece by 4 September. Named "Daniel" by the Hellenic National Weather Service, this cyclone brought severe thunderstorms to Greece, Turkey, and Bulgaria due to unstable atmospheric conditions and warm waters. Daniel traversed the Mediterranean Sea from 4 to 12 September 2023, bringing exceptionally heavy rainfall to Greece and Libya and triggering severe floods and mudslides. While moving south-southwest, Daniel stalled over the central Mediterranean, evolving into a subtropical storm by 7 September. By 9 September, Daniel transitioned into a tropical-like storm, making landfall in Libya on 10 September. Daniel dissipated into a low-pressure trough by 12 September (Hérincs, 2023; Normand and Heggy, 2024). Medicane Daniel brought intense winds of up to 120 km h^{-1} and delivered a total of 240 mm of rainfall over 25 h (Normand et al., 2024). It caused catastrophic flash flooding in Derna on 10 September 2023, as torrential rains overwhelmed the river's delta outlet. The flood destroyed large parts of the city's buildings, infrastructure, and bridges, resulting in 8.8 million tons of debris. In Derna alone, 10 % of houses were destroyed and 18.5 % damaged. In other cities, such as Susah, approximately 28 % of homes were destroyed, while Albayda, Al-Marj, and others also suffered heavy losses. Overall, the storm led to 5898 deaths, 8000 missing persons, 44 800 displaced individuals, and 18 838 homes damaged across Libya's northeastern coast, making it the deadliest African storm since 1900 (Hérincs, 2023; Normand et al., 2024; Katsanos et al., 2024).

3 Data and Methods

3.1 Data sources and products used

In this study, the best-track data for the medicane Daniel was obtained from the Zivipotty Cyclone Report database (https://zivipotty.hu/tcr.html, last access: 13 May 2026). Eddy identification was based on daily SLA fields sourced from the CMEMS. Specifically, the dataset SEALEVEL_EUR_PHY_L4_NRT_OBSERVATIONS_008_060, with a spatial resolution of 0.125°, was utilized. To detect and characterize the MHW, daily SST data from the NOAA Optimum Interpolation SST V2 dataset (Reynolds et al., 2007) were used. This dataset has a spatial resolution of 0.25° and covers the period from 1981 to the present. The key atmospheric variables, including total column water (which represents the sum of water vapor, liquid water, cloud ice, rain, and snow in a column extending from the surface of the Earth to the top of the atmosphere), total precipitation, vertically integrated moisture divergence, mean sea level pressure (MSLP), 10 m zonal and meridional wind com-

ponents, daily radiative fluxes of shortwave and longwave radiations, (denoted as Q_{SW} and Q_{LW} respectively), and turbulent heat fluxes of latent and sensible flux (denoted as Q_{lat} and Q_{sen} respectively) were retrieved from the ERA5 reanalysis (Hersbach et al., 2020). The surface net heat flux (Q_{net}) was derived from a combination of radiative and turbulent fluxes (Menna et al., 2023).

$$Q_{net} = Q_{SW} - Q_{LW} - Q_{lat} - Q_{sen} \quad (1)$$

High-resolution SLA observations were obtained from the SWOT Level 3 satellite product, which offers 2 km spatial resolution, provided by Archiving, Validation and Interpretation of Satellite Oceanographic data (AVISO; https://www.aviso.altimetry.fr/en/data, last access: 13 May 2026).

Lastly, biogeochemical variables such as chlorophyll, phytoplankton, nutrients, and dissolved oxygen were accessed via the CMEMS from the product MEDSEA_MULTIYEAR_BGC_006_008, available at a 4–5 km spatial resolution, and 1 h temporal resolution (https://doi.org/10.48670/mds-00374). Daily satellite-derived chlorophyll products (OCEANCOLOUR_MED_BGC_L4_NRT) with a spatial resolution of 1 km were used in this study (Volpe et al., 2019; Volpe et al., 2018; Berthon and Zibordi, 2004). These datasets are archived by the Copernicus Marine Service (https://doi.org/10.48670/moi-00298) and are provided by the Italian National Research Council (CNR, Rome, Italy), with data availability from January 2023 to the present. The multi-sensor product integrates observations from SeaWiFS, MODIS, MERIS, VIIRS, and OLCI, and includes key biogeochemical variables such as chlorophyll *a* (Chl *a*), diffuse attenuation coefficient at 490 nm, and primary production.

Despite their advantages, these datasets are subject to uncertainties arising from atmospheric correction errors, cloud contamination, aerosol effects, and reduced accuracy in optically complex coastal waters. In addition, the gap-filling procedure used to generate continuous fields may introduce smoothing in regions with persistent data gaps. Nevertheless, these products provide robust, high-resolution information on surface biogeochemical variability associated with cyclone-induced ocean processes.

3.2 Methods

In this study, we investigate the intensification, structure, and impacts of medicane Daniel. This section outlines the methodologies used to analyze the oceanic and atmospheric conditions associated with the event. The analysis focuses on key processes influencing cyclone formation and intensification, including the role of oceanic features such as WCEs and MHWs, the contribution of ocean heat content as a source of subsurface thermal energy, and atmospheric variables such as moisture and wind fields. The methods used for the identification of the sea eddies and MHWs, as well as the computation of ocean heat content, are described below.

3.2.1 Eddy and marine heatwave identification

Eddy identification in this study followed the approach of Jangir et al. (2021, 2023) and Sun et al. (2017), based on geostrophic balance equations relating SLA to geostrophic currents. Zonal (u) and meridional (v) velocity components were derived using Eqs. (2), (3), and (4):

$$u = -\frac{g}{f}\left(\frac{\mathrm{d}h}{\mathrm{d}y}\right) \quad (2)$$

$$v = \frac{g}{f}\left(\frac{\mathrm{d}h}{\mathrm{d}x}\right) \quad (3)$$

$$V^2 = u^2 + v^2 \quad (4)$$

where g is the acceleration caused by gravity, f is the Coriolis parameter, h is the SLA, and V is the geostrophic current speed.

Eddies were classified by analysing flow circulation and SLA patterns: anti-cyclonic circulation with a local SLA maximum indicated a WCE, while cyclonic circulation with a local SLA minimum indicated a cold-core eddy (CCE). This is consistent with previous findings, where WCEs in the Northern hemisphere exhibited clockwise (anti-cyclonic) rotation, while CCEs rotated counterclockwise (cyclonic). The relation between anti-cyclonic eddies and WCEs along the cyclone's path was also verified by inspecting SST anomalies with respect to a boxcar average.

MHWs were identified using the definition by Hobday et al. (2016) and the software developed by Zhao and Marin (2019) (https://github.com/ZijieZhaoMMHW/m_mhw1.0, last access: 13 May 2026). An MHW is defined as a period of at least 5 consecutive days during which the daily SST exceeds the seasonally varying 90th percentile, based on a climatological reference period (1983–2021). Events separated by less than 3 d are treated as a single MHW. Daily SST anomalies were computed by subtracting the daily climatology. MHW intensity was classified following Hobday et al. (2018) into four categories based on the metric θ, where θ represents the normalized SST anomaly relative to the climatological threshold. It is defined as:

$$\theta = \frac{\mathrm{SST} - \mathrm{SST}_{\mathrm{climatology}}}{\mathrm{SST}_{90\mathrm{th}_{\mathrm{percentile}}} - \mathrm{SST}_{\mathrm{climatology}}} \quad (5)$$

where SST is the daily sea surface temperature, $\mathrm{SST}_{\mathrm{climatology}}$ is the climatological mean SST, and $\mathrm{SST}_{90\mathrm{th}_{\mathrm{percentile}}}$ is the seasonally varying 90th percentile threshold. Based on this metric, MHW intensity is categorized as follows: moderate ($1 \leq \theta \leq 2$), strong ($2 \leq \theta \leq 3$), severe ($3 \leq \theta \leq 4$), and extreme ($\theta \geq 4$).

3.2.2 Computation of ocean heat content

We have also calculated the OHC to assess the role of subsurface heat accumulation in driving compound extreme events, such as the co-occurrence of MHWs and cyclones. Since the ocean acts as a key energy source for cyclones by supplying heat and moisture, the passage of a cyclone typically extracts heat from the upper ocean, leading to a decrease in OHC. In this study, OHC is defined as the vertically integrated thermal energy from the surface down to the depth of the 20 °C isotherm (a proxy for the thermocline layer). The OHC was computed for the medicane using the following formulation (Eq. 6):

$$\mathrm{OHC} = \int_{h1}^{h2} \rho C_\mathrm{p} T \, \mathrm{d}z \tag{6}$$

where ρ is the density of the seawater, C_p is the specific heat capacity of the seawater at constant pressure, p, $h1$ is the surface, $h2$ is the bottom depth, and T is the temperature in °C. This approach allows us to quantify how much thermal energy is available in the upper ocean to potentially intensify cyclones and how this energy is depleted following cyclone passage.

3.2.3 Computation of Ekman pumping

Ekman pumping was computed using the wind stress components $\tau = (\tau_x, \tau_y)$ from ERA5, namely Eastward Wind Stress (EWSS) and Northward Wind Stress (NSSS), which is available for $0.25° \cdot 0.25°$ and hourly temporal resolution. To compute the wind stress curl ($\nabla \cdot \tau$), the spatial derivatives of wind stress are used, and it is computed using Eq. (7):

$$\mathrm{curl}\,(\tau) = \frac{\partial \tau_y}{\partial x} - \frac{\partial \tau_x}{\partial y} \tag{7}$$

The wind stress curl ($\nabla \cdot \tau$) was calculated using finite-difference estimates of spatial gradients on a latitude-longitude grid, with grid spacing converted to metric units. No additional smoothing was applied to the wind stress fields prior to curl computation. Then, the Ekman pumping velocity (w_e), introduced by Stern (1965) to account for the effect of the ocean currents on upwelling, is calculated using Eq. (8):

$$w_\mathrm{e} = \frac{1}{\rho} \times \mathrm{curl}\left(\frac{\tau}{f+\zeta}\right) \tag{8}$$

This vertical velocity reflects the upwelling (positive w_e) or downwelling (negative w_e) of water, and is a crucial mechanism through which cyclones influence oceanic nutrient transport, mixing, and biological productivity (Li et al., 2021). Here, the relative vorticity (ζ) was computed from the zonal (u) and meridional (v) components of the surface current, as given in Eq. (9):

$$\zeta = \frac{\partial v}{\partial x} - \frac{\partial u}{\partial y} \tag{9}$$

The Ekman transport vector components were computed from the wind stress and Coriolis parameter as:

$$M_x = \frac{\tau_y}{\rho\,(f+\zeta)} \tag{10}$$

$$M_y = \frac{\tau_x}{\rho\,(f+\zeta)} \tag{11}$$

where ρ is seawater density, and f is the Coriolis parameter (dependent on latitude). The vector field $M = (M_x, M_y)$ was visualized using quiver plots to reveal the spatial structure and directional response of Ekman transport to cyclone wind forcing.

3.2.4 Computation of various properties along the track of medicane Daniel

To estimate the medicane's characteristic MSLP and wind speed along the cyclone track, we applied Cressman averaging (Cressman, 1959). Once the cyclone center was identified, a spatial average within a 2° radius around the center, weighted by inverse square distance, was computed for MSLP and wind speed. This method captures changes within a 2° radius of the cyclone centre, while regions outside this radius are not included. Similarly, daily MHW and high-pass filtered (500 km radius) SST and OHC anomalies, along with their along-track evolution during medicane Daniel, were calculated using a 2° search radius and the Cressman interpolation technique. This analysis allows quantification of the relative extremity of the oceanic conditions encountered during intensification. The approach was used to assess variations in cyclone intensity along its path and has been widely employed in previous studies (Jangir et al., 2023).

4 Results and discussion

In this section, we present the results of our study on medicane Daniel, focusing on two primary aspects. First, we analyze the influence of pre-existing oceanic conditions, specifically WCEs and MHW conditions, on the cyclone's intensification. Second, we investigate the medicane's impact on ocean biogeochemistry, particularly the observed increase in surface productivity as indicated by enhanced biogeochemical variables. Our findings also explore the physical mechanisms behind these changes, highlighting the interactions between the ocean and atmosphere throughout the lifecycle of medicane Daniel.

4.1 Role of oceanic features in intensification of medicane Daniel

Figure 1a–b shows the SLA along the medicane's track. At first, the medicane passed over a cluster of three anticyclonic eddies between 4 and 6 September, presumably contributing to its intensification (Jangir et al., 2023). This intensification

between 8 and 10 September was also supported by the presence of a moderate MHW, as shown in Fig. 1c–e (see also Fig. S1 in the Supplement). Furthermore, just before making landfall, the medicane arrived in a region characterized mostly by anticyclonic mesoscale WCE activity (Fig. 1f–h). OHC anomaly shown in Fig. 1i–k indicates higher heat content in the southern part of the domain close to landfall location, also supporting the intensification of the medicane. In addition to the maps in panels (c)–(k) of Fig. 1, the analysis was carried out by computing MHW, SST, and OHC anomalies at each 6 h track position (Fig. 1l–n), with particular emphasis on the maximum cyclone intensity (Max-CI) location. We observed from the analysis that the maximal values of MHW (~ 0.6), SST ($\sim 0.83\,^{\circ}\mathrm{C}$), and OHC ($\sim 16.30\,\mathrm{KJ\,cm^{-2}}$) anomalies occurred in the last 2 d before Max-CI, indicating that medicane Daniel intensified over thermodynamically favourable conditions that were among the most anomalous along its track.

The combination of two extreme oceanic preconditions, namely the WCE and the MHW, together with high absolute values of OHC at the intensification site near the coastal region, may have contributed to the deadly outcome of this medicane. Rathore et al. (2022) and Jangir et al. (2024) highlighted the critical role of sudden intensification in Cyclone Amphan over the Indian Ocean and medicane Ianos over the Mediterranean Sea, respectively, in the presence of MHWs along their paths. The findings of the current study are consistent with these observations, demonstrating that while cyclone genesis and intensification can occur independently of such features, the presence of WCEs and MHWs may enhance the rate and magnitude of intensification over a shorter time.

Figure 1 also highlights the potential importance of ocean characteristics such as WCEs and MHWs in cyclone intensification, indicating that cyclone intensity increased in the presence of WCEs and MHWs. This behavior is similar to how cyclones in other ocean basins react to changes in intensification factors related to underlying eddies (Ali et al., 2007; Lin et al., 2013; Jangir et al., 2021, 2023). When a cyclone encounters a WCE, the negative feedback loop between cyclone intensity and SST diminishes. Normally, cyclones extract heat from the ocean, resulting in surface cooling due to enhanced mixing and evaporation, which acts to reduce cyclone intensity. However, if a WCE or MHWs are present, the high SST persists longer, intensifying the cyclone and reducing the negative feedback effect (Bender et al., 1993; Jangir et al., 2024).

Furthermore, atmospheric cyclones draw a significant portion of their energy from warm, deep ocean waters; therefore, quantifying the amount of this warm, deep water provides a more accurate measure of the energy available to the storm. OHC serves as this metric, indicating how much warm water a cyclone can convert into energy. Studies have shown that OHC is a far superior predictor compared to SST alone (Wada and Usui, 2007; Sharma and Ali, 2014; Lin et al., 2013; Law, 2011). Analysis of the OHC revealed a significant amount of OHC at the intensification locations, providing a favorable upper-ocean thermal reservoir for medicane Daniel to intensify. Approximately $120\,\mathrm{KJ\,cm^{-2}}$ of heat was available from 4 to 9 September, even before the cyclone's intensification (Fig. 1i–k and Fig. S2). This accumulated heat at the intensification location is attributed to the presence of the WCE and the MHW, which decreases after the passage of the medicane on 11 and 12 September 2023 (Fig. S2). The presence of heat in the form of SST anomaly (Fig. 1f–h) and OHC anomaly (Fig. 1i–k) along the path of medicane maintains intensity by reducing negative feedback that occurs due to the passage of the cyclone (Jangir et al., 2023; Jangir et al., 2024).

4.2 The role of atmospheric precursors in the intensification of medicane Daniel

The MSLP and wind speed, computed using the Cressman averaging method (Cressman, 1959) along the cyclone's track, are shown in Fig. 2a. The MSLP indicates moderate intensification from 1006 to 1002 hPa when the storm passes over the WCE on 5 September 2023 (Fig. 2a). Subsequently, from 6 to 7 September 2023, the medicane passes over a CCE region, and its intensity is reduced to 1004 hPa. Upon reaching the vicinity of Libya's coast on 8 September 2023, it quickly intensified. An additional WCE was present in the vicinity of the cyclone's path at that time, potentially further contributing to its fast intensification. This fast intensification is indicated by a drop in the MSLP and a sudden increase in wind speed near the eddy and MHW location (Fig. 2a). The cutoff low, which was supported by high net heat flux, persisted for 2 d (Figs. 2b–d, S3), even after the cyclone made landfall in Libya.

Moisture processes play an equally important role in cyclone intensification. Their importances been demonstrated in previous studies by Jangir et al. (2023) and Pytharoulis et al. (2018), emphasizing that elevated SST in the form of WCE or MHW is essential for providing moisture to a medicane via surface fluxes, enhancing convection. Additionally, Jangir et al. (2024) highlighted the importance of moisture convergence in the intensification of cyclones and increasing total associated precipitation. Thus, motivated by these findings, we focus in this study on the causes of the intensification of the medicane Daniel and the extreme flood that occurred during the event.

The analysis of moisture convergence (i.e., mean vertically integrated moisture divergence) showed a pattern of moisture convergence along the cyclone's path. Notably, this convergence coincides with the eddy location at the intensification location on 9 September 2023 (Fig. S4). This alignment suggests that the eddy supplied the moisture needed for the cyclone's intensification. The interaction between the eddy and the medicane likely enhanced moisture availability, contributing to the storm's strengthening at that specific point in

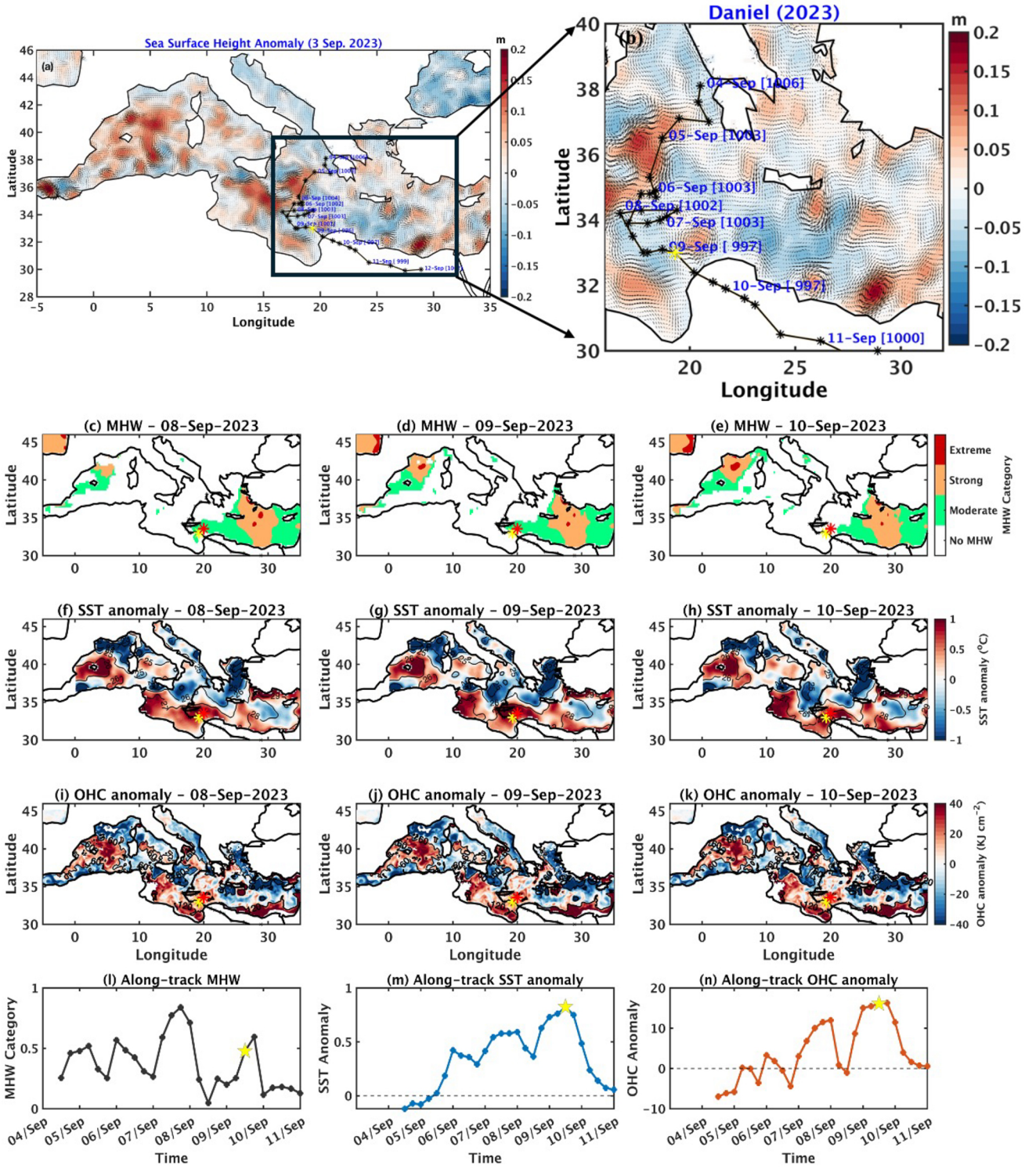

Figure 1. (a, b) Sea level anomaly (shading) with geostrophic currents (arrows). The medicane track is overlaid on **(c–e)** marine heatwave (MHW), **(f–h)** sea surface temperature (SST) anomalies (500 km radius high pass filter), and **(i–k)** ocean heat content (OHC) anomalies (500 km radius high pass filter). In panels **(f)**–**(k)**, absolute values are indicated by contours. Panels **(l)**–**(n)** show along-track values of MHW, SST, and OHC anomalies. The yellow stars **(a–k)** and Pentagon **(l–n)** mark the location of maximum cyclone intensity (Max-CI), while the red pentagons mark the Max-CI location defined by the minimum mean sea level pressure. The red star marker in panels **(c)**–**(k)** indicates the position of the WCE. Dates for each panel are shown along the track.

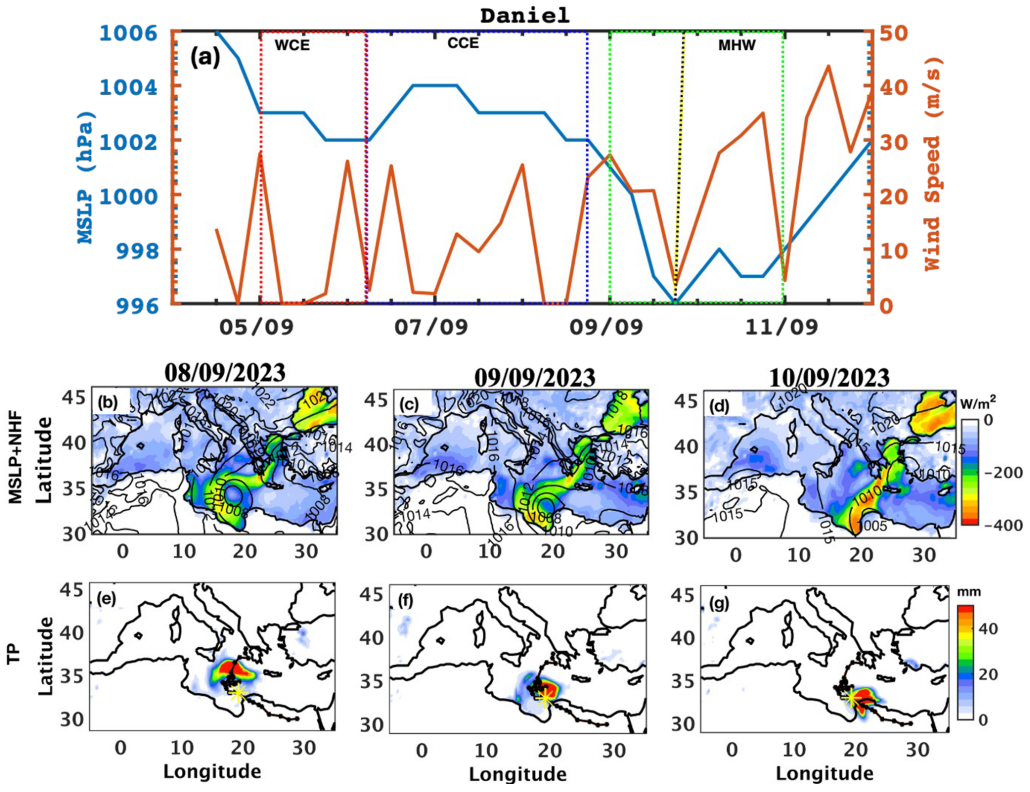

Figure 2. (a) Mean sea level pressure (MSLP), and wind speed computed using the Cressman average along the track of the medicane Daniel. The red, blue, and green boxes indicate the locations of the warm-core eddy (WCE), cold-core eddy (CCE) and marine heatwave (MHW), respectively. The medicane track is overlaid on **(b–d)** the daily mean of MSLP (contours) net heat fluxes (shading; positive downward), and on **(e–g)** total precipitation for 8–10 September 2023. The yellow star indicates the location of maximum intensification (Max-CI).

it's path. Additionally, the total column water was notably high at the WCE and MHW locations. While this total water was present before the intensification location as well, it converged around the eddy at the intensification location (Fig. S5), leading to substantial precipitation in that area (Figs. 2e–g and S6). The severe precipitation near the coastal region highly coincides with the WCE and MHW. The WCE's influence intensified the cyclone by providing additional moisture and heat, leading to heavy rainfall. This heavy precipitation, concentrated near the coast, exacerbated the storm's impact, severely damaging the affected areas.

4.3 SWOT satellite data

The SWOT mission offers high-resolution sea surface height anomaly or SLA data with unprecedented spatial detail, enabling precise detection of mesoscale and sub-mesoscale ocean features, such as eddies and fronts (Morrow et al., 2019). This can be valuable for studying cyclones, which interact strongly with oceanic eddies that influence storm intensity. Unlike traditional altimeters, SWOT's wide-swath coverage enables improved detection of mesoscale and sub-mesoscale eddies, frontal gradients, and filaments that regulate ocean heat distribution and air-sea exchanges. These features are often underrepresented in low-resolution datasets, limiting their ability to capture localized processes such as eddy-cyclone interactions and cyclone-induced mixing. By improving the detection of these fine-scale physical structures, SWOT also provides a framework for interpreting biogeochemical responses. While coarse datasets show bulk chlorophyll changes, SWOT helps identify localized regions of enhanced mixing and upwelling that drive nutrient supply and biological variability. This allows for a clearer linkage between physical forcing and biogeochemical response. Overall, SWOT overcomes key limitations of conventional altimetry by preserving high-frequency spatial gradients, enabling a more accurate representation of the ocean state during extreme events such as medicane Daniel.

Here we show the SWOT swath passing over the location of the eddies along the track of medicane Daniel (Fig. 3). In Fig. 3a–b, the eddy initially appears small and low intensity in the CMEMS, and the cyclone is observed nearby. However, SWOT data reveal a more intense and extensive eddy structure than CMEMS, with the cyclone positioned directly above it. These findings report the value of SWOT observations in capturing fine-scale oceanic features and dynamics, offering critical insights into cyclone-eddy interactions.

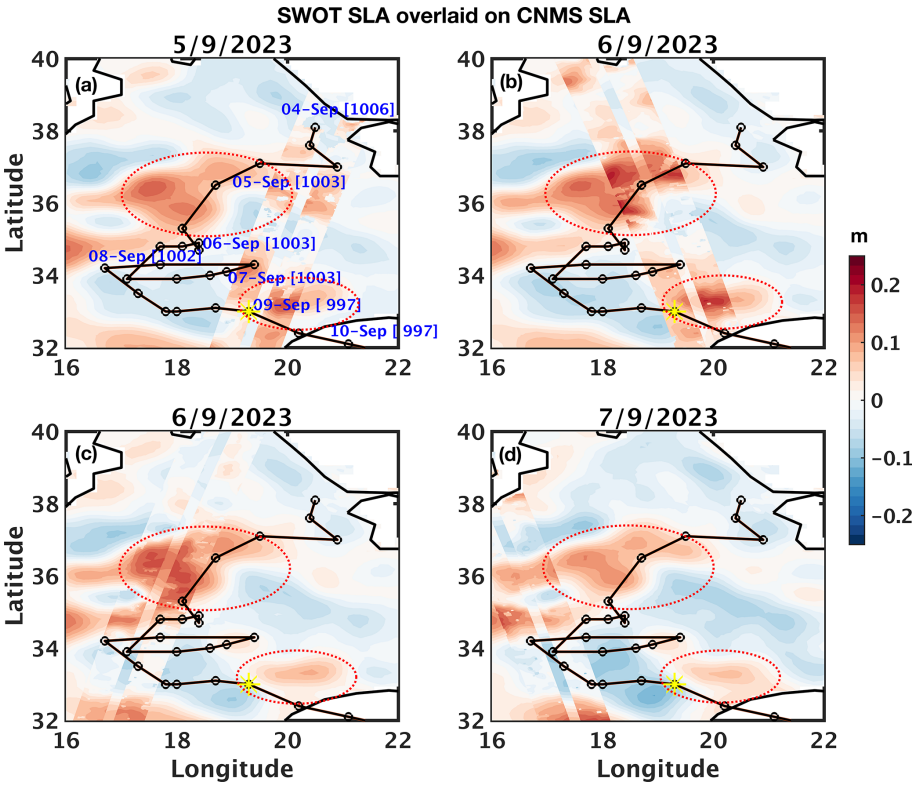

Figure 3. (a-d) The SWOT sea level anomaly (SLA) swath (2 km resolution) overlaid on SLA from CMEMS (12.5 km spatial resolution). The dates shown above each panel correspond to the periods of SWOT swath data availability.

4.4 Impact of medicane Daniel on ocean biogeochemistry

To investigate the impact of the medicane on oceanic physical (temperature and salinity) and biogeochemical properties (i.e., chlorophyll *a*, phytoplankton, nitrate and phosphate, and oxygen concentration), we analyzed vertical profiles of key variables along the cyclone's track. The analysis focused on differences between 2 d after the cyclone's passage, minus 2 d before (Fig. 4a–g). The results reveal a notable decrease in temperature along the cyclone path, with a general strong cooling along its path except for a short pause in the cold SST anomaly region in the morning of the 8th (Fig. 1n). This region was also relatively outside the MHW domain (Fig. 1l). The salinity also decreases on the surface presumably due to a massive influx of freshwater from heavy rainfall, again, except for the morning of the 8th, in which the cyclone was outside the influence of WCEs and MHW (Fig. 4b). In contrast, at the subsurface, Chl *a* and phytoplankton concentrations exhibit a marked dipole (Fig. 4c–d), while nutrients increase (Fig. 4e–f) and oxygen decreases (Fig. 4g). This biological response can be attributed to cyclone-induced Ekman pumping upwelling and high subsurface vertical mixing. Enhanced nutrient availability at the subsurface layer can persist into the mixed layer, allowing for sufficient sunlight, and together with elevated oxygen concentrations (associated with surface cooling), may foster increased surface Chl *a* and phytoplankton biomass. Signs of this can be seen in the MHW region, where higher Chl *a* concentrations reach the surface. But, unlike previous results (Jangir et al., 2026), medicane Daniel only shows an increase in Chl *a* at the surface in the MHW region.

Profiles of temperature and Chl *a* at the maximum cyclone intensity (Max-CI) location and time (Fig. 4h–i) reveal general cooling after the passage of the cyclone. The deep chlorophyll maximum (DCM) was located far below the mixed layer depth, at around 140 m depth. The subsurface crossings between the profiles and the relatively stationary location of the DCM in Fig. 4i indicate that out of the two processes mentioned above, namely cyclone-induced upwelling and high subsurface vertical mixing, only cyclone-induced subsurface mixing can explain the change. Subsurface mixing mechanism is typically much slower than turbulence in the mixed layer, but under storm conditions may become comparable. The gradual subsurface increase in Chl *a*, as opposed to the vertical line observed in the mixed layer, indicates weaker but comparable turbulence below the mixed layer.

Figure 4i shows the change in subsurface profiles at the time and location of Max-CI, situated on the periphery of a WCE. To further investigate the underlying mechanisms and compare the medicane's impact on both WCEs and

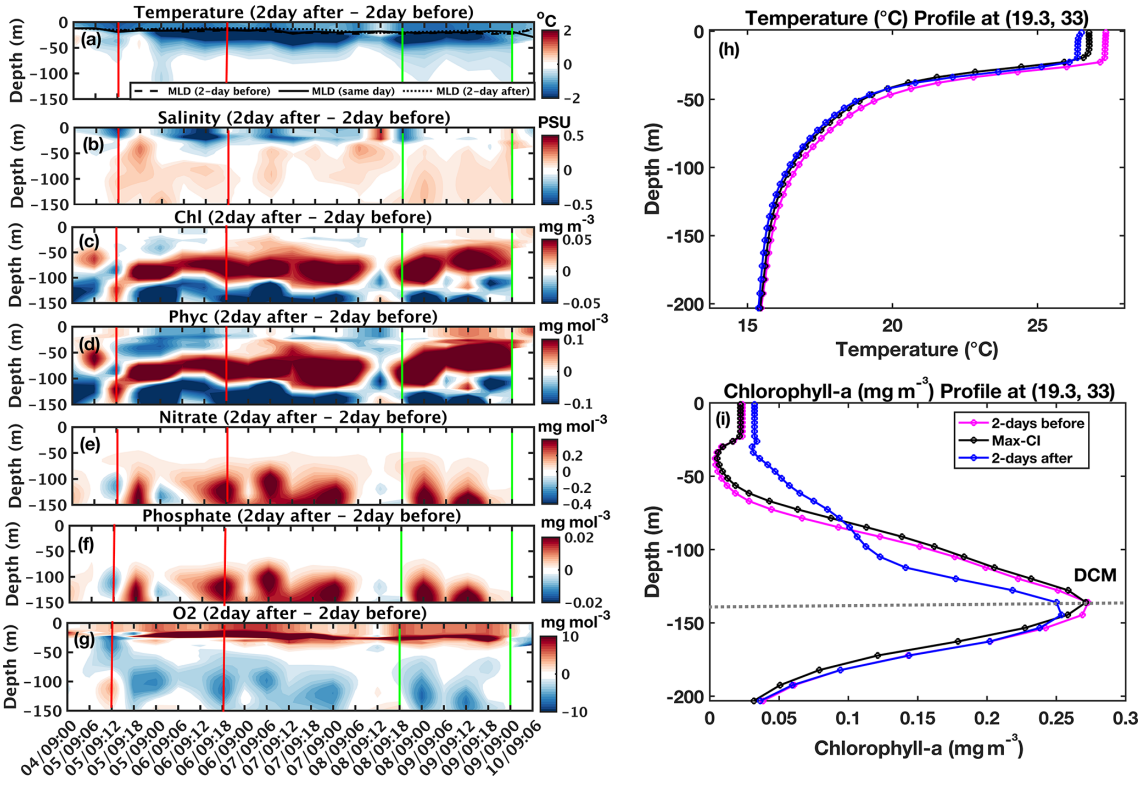

Figure 4. Profiles of physical **(a-d)** and biogeochemical **(e-g)** variables along the track of medicane Daniel. Panels **(a)**–**(g)** show the difference between 2 d after and 2 d before the event. Red and green vertical lines in panels **(a)**–**(g)** delineate the location of the warm-core eddy (WCE) and marine heatwave (MHW) along the track, respectively. The black line in the temperature profile indicates the mixed layer depth. Panels **(h)**–**(i)** represents the temperature and chlorophyll profiles at the Maximum Cyclone Intensity (Max-CI) location, 2 d before and after the Max-CI location.

CCEs, vertical cross-sections across the main center of the WCE and adjacent CCE region were analyzed during the pre-storm, during storm, and post-storm phases (Fig. 5). These cross-sections reveal notable eddy-dependent subsurface changes associated with the passage of the medicane. As expected, during and after the passage of the storm, significant surface cooling is observed in Fig. 5 (panels b–d and h–i). In addition to the cooling observed within the mixed layer, three distinct circular-like cooling patterns are evident immediately beneath it. These may indicate a secondary circulation starting at the deep subsurface (below 200 m), which transfers deep cold water to the layers below the mixed layer. In this case, the two patterns on the right indicate an upwelling cell at the WCE boundaries (green arrows in Fig. 5i) and another at the CCE center (purple arrow in Fig. 5i). These circulation cells also create the dipole pattern in the Chl *a* inside the WCE and the CCE (Fig. 5e–g and j–k).

To explore the dynamical mechanisms, Fig. 6 shows vertical profiles from 1 to 15 September 2023 of Chl *a* at two locations along the same line as in Fig. 5a, one inside the CCE (panel a) and the other inside the WCE (panel b). Before the arrival of the medicane (1–5 September), the DCM within the CCE was shallower than in the WCE, consistent with the typical vertical structure of these eddies. The DCM in both eddies remains relatively stable until the cyclone approaches the region. As the medicane approaches the eddies, it intensifies the CCE while diminishing the WCE, which, as expected from theory (e.g., Klein and Lapeyre, 2009), supports eddy-induced upwelling. Indeed, during the storm, the DCM is lifted upward in both cases from 5 to 9 September. Yet, the DCM inside the WCE is exhibited significantly greater shoaling than inside the CCE (~ 40 m in the WCE relative to ~ 15 m in the CCE). The more pronounced response in the WCE likely stems from lower thermal stratification and higher surface wind stress curl that contribute to cyclone-induced Ekman pumping upwelling. Only a few days later, the DCM inside the WCE partially starts to restore its pre-storm condition. The DCM inside the CCE quickly drops back down and even overshoots its depth relative to pre-storm conditions, which can be explained by its stronger stratification and resulting buoyancy restoring force. In addition, we found that cyclone-induced upwelling alone cannot explain the DCM increase in both the WCE and CCE (Fig. 6c), which indicates an increase of about 10–15 m during the medicane influence (5–9 September). Therefore, we

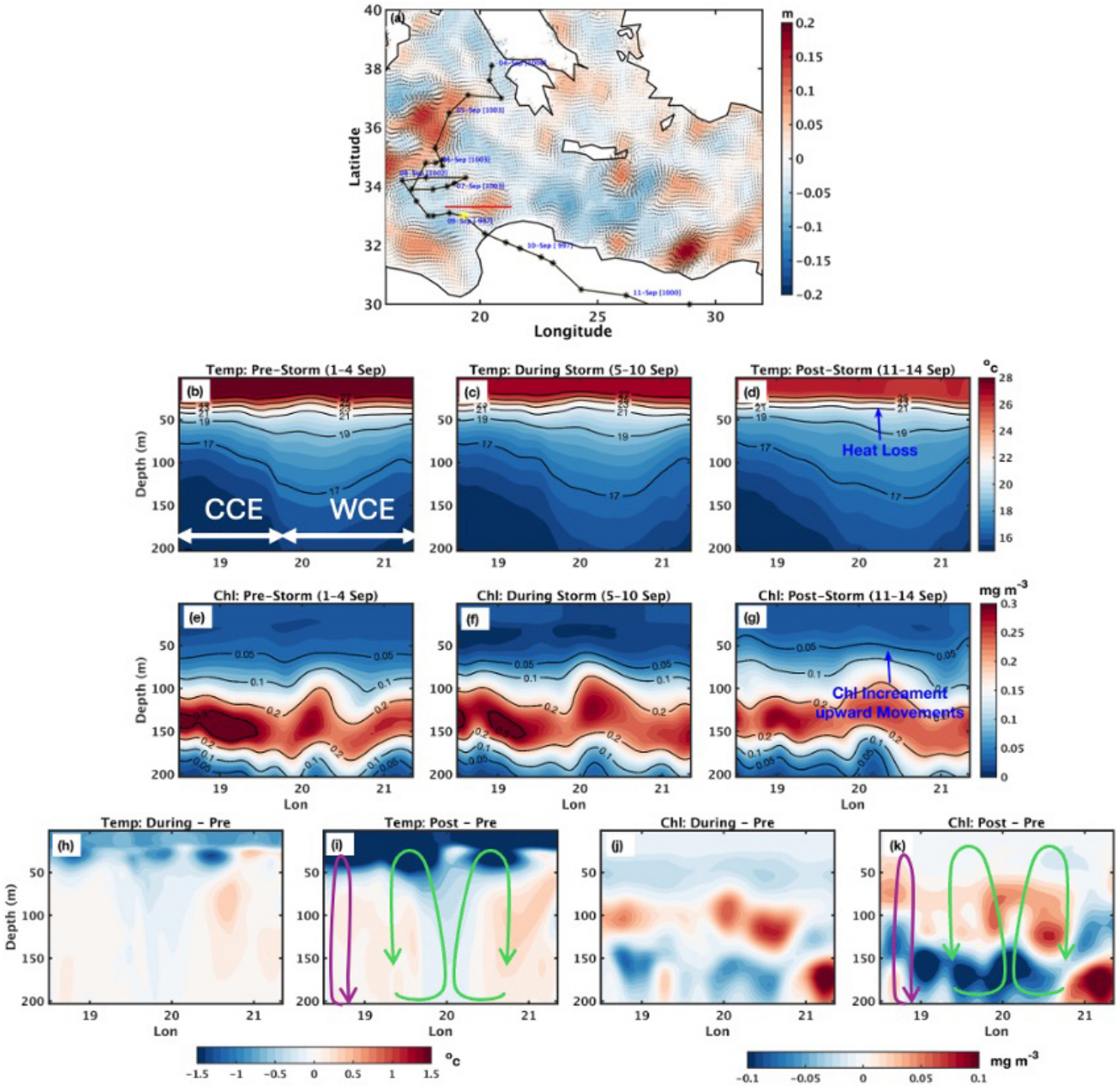

Figure 5. **(a)** Sea level anomaly with a red line indicating the section across the second warm-core eddy (WCE) used in subsequent panels. **(b–d)** Temperature profiles and isotherms before, during, and after the medicane along this section. **(e–g)** Chlorophyll *a* profiles before, during, and after the medicane along the same section. **(h–i)** Temperature differences (during-storm minus pre-storm, and post-storm minus pre-storm). **(j)–(k)** Same as **(h)–(i)**, but for chlorophyll *a*. Green arrows denote the location of a secondary circulation cell, and the purple arrow indicates subsurface mixing.

conclude that the upwelling may have also been influenced by isopycnal adjustment triggered by the medicane.

Subsurface mixing similar to what was shown under the medicane at Max-CI (Fig. 4i), seems to play a role also here. This role can be indicated by the crossing of the Chl *a* profiles during the storm (5–9 September) with the profiles after the storm (10–15 September) between MLD (~ -20 m) and the DCM (~ -130 m). However, here, it seems to complement upwelling and to play a more important role at the WCE (as expected, since in general wind stress is higher above WCEs). Also, satellite-based surface observations (Fig. 6d) indicate higher Chl *a* above the WCE region, which may be explained by the closer-to-the-surface DCM and stronger cyclone-induced upwelling and vertical mixing.

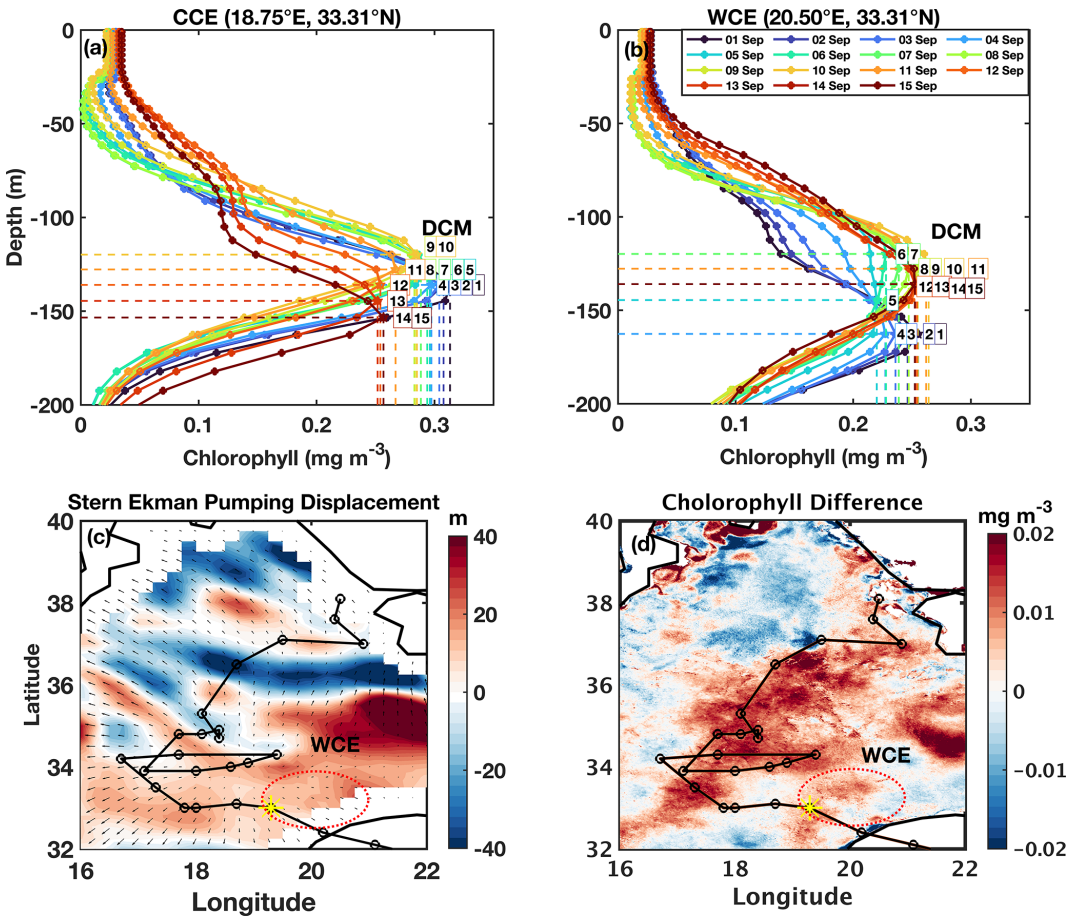

Figure 6. Chlorophyll *a* profiles from 1 to 15 September 2023 at the cold-core eddy (CCE; **a**) and warm-core eddy (WCE; **b**) locations. **(c)** Cumulative Ekman pumping displacement for 5–9 September 2023, with arrows indicating the transport vector during the cyclone. **(d)** Satellite chlorophyll *a* (2 km spatial resolution) before and after medicane Daniel. The red dotted ellipse indicates the location of the WCE, and the yellow star denotes the location of maximum cyclone intensity (Max-CI).

5 Conclusions

This case study provides comprehensive insights into the intensification and impacts of medicane Daniel, which developed over the Mediterranean Sea in September 2023. The findings show the significant role of oceanic and atmospheric variables in cyclone intensification, particularly the presence of WCE and MHW (Fig. 7). These oceanic features reduced the negative feedback loop between cyclone intensity and SST, allowing the cyclone to maintain and even increase it's intensity. This study also highlighted the importance of OHC in providing the energy necessary for cyclone intensification, with approximately 120 KJ cm^{-2} of heat available at the intensification location over the WCE and MHW. Additionally, the convergence of moisture at the locations of the WCE and MHW, combined with the elevated total water column, contributed to the heavy precipitation observed in the coastal areas in Libya.

This study highlights the critical role of high-resolution SWOT data in advancing our understanding of air-sea interaction processes. While CMEMS data, with its coarser spatial resolution, suggests the presence of a weak eddy near the cyclone intensification region, SWOT's finer 2 km resolution reveals a high-intensity WCE precisely aligned with the cyclone's path. This enhanced detection capability provides a more accurate illustration of eddy characteristics and their influence on cyclone dynamics. Furthermore, satellite-derived Chl *a* data indicate an enhanced bloom over the WCE location, supported by positive Ekman pumping values. These high values indicate cyclone-induced upward movement of water from deeper layers to the surface, bringing cold, nutrient-rich water to the surface, and boosting ocean productivity.

Subsurface profiles of physical and biogeochemical properties show a notable temperature decrease above the mixed layer depth, particularly over the WCE and MHW regions. The passage of the cyclone triggers vertical mixing, leading to an increase in surface nutrient concentrations. Combined with sufficient sunlight in the euphotic zone, this promotes a surge in surface Chl *a* and phytoplankton produc-

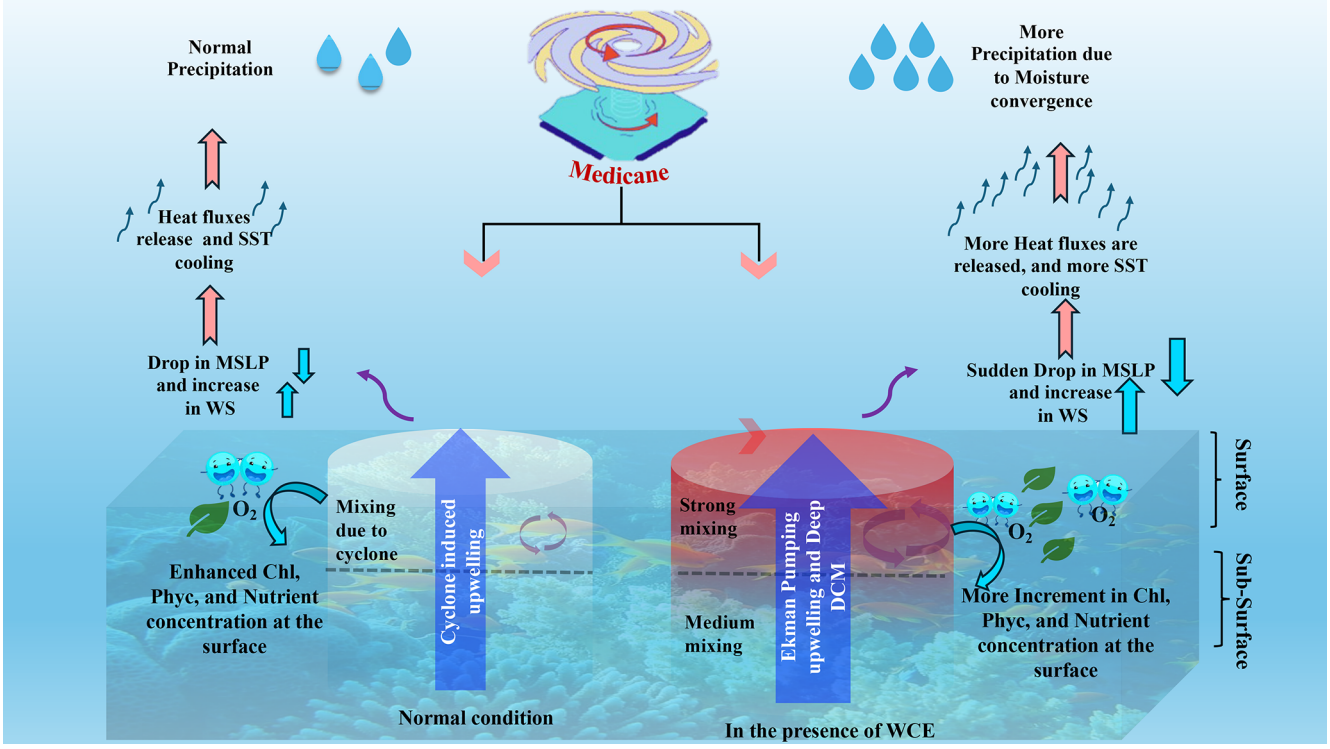

Figure 7. Schematic illustrating the process associated with cyclone intensification over warm-core eddy and marine heatwave, and their impact on ocean biogeochemistry.

tivity. Cross-sectional analysis further reinforces these findings: a clear upward shift in isotherms following the cyclone indicates heat loss and active upwelling over the WCE. Concurrently, the Chl *a* sections display an upward displacement and intensification of Chl *a* concentrations, confirming the strong biogeochemical response induced by the cyclone's passage over the WCE region.

In conclusion, the study of medicane Daniel emphasizes the need for a deeper understanding of both oceanic and atmospheric factors in predicting and mitigating the impacts of such cyclones in the Mediterranean region. The findings suggest that, similar to tropical cyclones in other ocean basins, medicanes are significantly influenced by the interplay of oceanic heat content, eddies, and atmospheric dynamics. These factors are responsible for the intensification of the cyclone and the destruction caused by the medicane.

Data availability. Data can be Archived from the links below:

- https://doi.org/10.48670/mds-00374: Cossarini et al., 2021; https://doi.org/10.25423/CMCC/MEDSEA_MULTIYEAR_BGC_006_008_MEDBFM3 (Teruzzi et al., 2021a), https://doi.org/10.25423/CMCC/MEDSEA_MULTIYEAR_BGC_006_008_MEDBFM3I (Teruzzi et al., 2021b),
- https://doi.org/10.48670/moi-00298: Volpe et al. (2018, 2019), Berthon and Zibordi (2004),
- https://zivipotty.hu/tcr.html (last access: 13 May 2026),
- https://www.aviso.altimetry.fr/en/data (last access: 13 May 2026).

Supplement. The supplement related to this article is available online at https://doi.org/10.5194/bg-23-4271-2026-supplement.

Author contributions. B.J. contributed to the conceptualization of the study, data curation, formal analysis, and writing of the original draft. E.S. served as the project investigator, contributed to conceptualization, provided resources and software support, supervised the research, and contributed to review, and editing, as well as funding acquisition.

Competing interests. The contact author has declared that neither of the authors has any competing interests.

Disclaimer. Publisher's note: Copernicus Publications remains neutral with regard to jurisdictional claims made in the text, published maps, institutional affiliations, or any other geographical representation in this paper. The authors bear the ultimate responsibility for providing appropriate place names. Views expressed in the text are those of the authors and do not necessarily reflect the views of the publisher.

Acknowledgements. The authors acknowledge the data-providing agencies (i.e., CMEMS, AVISO) for providing data free of cost.

Financial support. This research has been supported by the Israel Science Foundation (grant no. 2228/21).

Review statement. This paper was edited by Tina Treude and reviewed by three anonymous referees.

References

Ali, M. M., Jagadeesh, P. S. V., and Jain, S.: Effects of eddies on Bay of Bengal cyclone intensity, Eos Trans. AGU, 88, 93–95, https://doi.org/10.1029/2007EO080001, 2007.

Archer, M., Wang, J., Klein, P., Dibarboure, G., and Fu, L. L.: Wide-swath satellite altimetry unveils global submesoscale ocean dynamics, Nature, 640, 691–696, https://doi.org/10.1038/s41586-025-08722-8, 2025.

Avolio, E., Fanelli, C., Pisano, A., and Miglietta, M. M.: Unveiling the relationship between Mediterranean tropical-like cyclones and rising Sea Surface Temperature, Geophys. Res. Lett., 51, https://doi.org/10.1029/2024GL109921, 2024.

Bender, M. A., Ginis, I., and Kurihara, Y.: Numerical simulations of tropical cyclone-ocean interaction with a high-resolution coupled model, J. Geophys. Res., 98, 23245–23263, https://doi.org/10.1029/93JD02370, 1993.

Berthon, J.-F. and Zibordi, G.: Bio-optical relationships for the northern Adriatic Sea, Int. J. Remote Sens., 25, 1527–1532, 2004.

Chen, Y., Pan, G., Mortimer, R., and Zhao, H.: Possible Mechanism of Phytoplankton Blooms at the Sea Surface after Tropical Cyclones, Remote Sens., 14, 6207, https://doi.org/10.3390/rs14246207, 2022.

Cherif, S., Doblas-Miranda, E., Lionello, P., Borrego, C., Giorgi, F., Iglesias, A., Jebari, S., Mahmoudi, E., Moriondo, M., Pringault, O., Rilov, G., Somot, S., Tsikliras, A., Vila, M., and Zittis, G.: Drivers of change. In Climate and environmental change in the Mediterranean Basin – current situation and risks for the future, First Mediterranean Assessment Report, Union for the Mediterranean, Plan Bleu, UNEP/MAP, 59–128, https://doi.org/978-2-9577416-0-1, 2020.

Chowdhury, R. R., Prasanna Kumar, S., Narvekar, J., and Chakraborty, A.: Back-to-back occurrence of tropical cyclones in the Arabian Sea during October–November 2015: Causes and responses, J. Geophys. Res.-Oceans, 125, https://doi.org/10.1029/2019JC015836, 2020.

Claud, C., Alhammoud, B., Funatsu, B. M., and Chaboureau, J.-P.: Mediterranean hurricanes: large-scale environment and convective and precipitating areas from satellite microwave observations, Nat. Hazards Earth Syst. Sci., 10, 2199–2213, https://doi.org/10.5194/nhess-10-2199-2010, 2010.

Cossarini, G., Feudale, L., Teruzzi, A., Bolzon, G., Coidessa, G., Solidoro C., Amadio, C., Lazzari, P., Brosich, A., Di Biagio, V., and Salon, S.: High-resolution reanalysis of the Mediterranean Sea biogeochemistry (1999–2019), Frontiers in Marine Science, Front. Mar. Sci., 8, 741486, https://doi.org/10.3389/fmars.2021.741486, 2021.

Cressman, G. P.: An operational objective analysis scheme, Mon. Weather Rev., 87, 367–374, https://doi.org/10.1175/1520-0493(1959)087<0367:aooas>2.0.co;2, 1959.

Dutta, D., Mani, B., and Dash, M. K.: Dynamic and thermodynamic upper-ocean response to the passage of Bay of Bengal cyclones "Phailin" and "Hudhud": a study using a coupled modelling system, Environ. Monit. Assess., 191 (Suppl. 3), 808, https://doi.org/10.1007/s10661-019-7704-9, 2019.

Emanuel, K.: Genesis and maintenance of "Mediterranean hurricanes", Adv. Geosci., 2, 217–220, https://doi.org/10.5194/adgeo-2-217-2005, 2005.

Fita, L., Romero, R., Luque, A., Emanuel, K., and Ramis, C.: Analysis of the environments of seven Mediterranean tropical-like storms using an axisymmetric, nonhydrostatic, cloud resolving model, Nat. Hazards Earth Syst. Sci., 7, 41–56, https://doi.org/10.5194/nhess-7-41-2007, 2007.

Flaounas, E., Raveh-Rubin, S., Wernli, H., Drobinski, P., and Bastin, S.: The dynamical structure of intense Mediterranean cyclones, Clim. Dynam., 44, 2411–2427, https://doi.org/10.1007/s00382-014-2330-2, 2015.

Flaounas, E., Davolio, S., Raveh-Rubin, S., Pantillon, F., Miglietta, M. M., Gaertner, M. A., Hatzaki, M., Homar, V., Khodayar, S., Korres, G., Kotroni, V., Kushta, J., Reale, M., and Ricard, D.: Mediterranean cyclones: current knowledge and open questions on dynamics, prediction, climatology and impacts, Weather Clim. Dynam., 3, 173–208, https://doi.org/10.5194/wcd-3-173-2022, 2022.

Flaounas, E., Dafis, S., Davolio, S., Faranda, D., Ferrarin, C., Hartmuth, K., Hochman, A., Koutroulis, A., Khodayar, S., Miglietta, M. M., Pantillon, F., Patlakas, P., Sprenger, M., and Thurnherr, I.: Dynamics, predictability, impacts and climate change considerations of the catastrophic Mediterranean Storm Daniel (2023), Weather Clim. Dynam., 6, 1515–1538, https://doi.org/10.5194/wcd-6-1515-2025, 2025.

Flocas, H. A.: Diagnostics of cyclogenesis over the Aegean sea using potential vorticity inversion, Meteorol. Atmos. Phys., 73, 25–33, https://doi.org/10.1007/s007030050061, 2000.

González-Alemán, J. J., Pascale, S., Gutierrez-Fernandez, J., Murakami, H., Gaertner, M. A., and Vecchi, G. A.: Potential increase in hazard from Mediterranean hurricane activity with global warming, Geophys. Res. Lett., 46, 1754–1764, https://doi.org/10.1029/2018GL081253, 2019.

Hérincs, D.: Tropical Storm Daniel: Mediterranean tropical cyclone report (7–10 September 2023), https://zivipotty.hu/2023_daniel.pdf (last access: 13 May 2026), 2023.

Hersbach, H., Bell, B., Berrisford, P., Hirahara, S., Horányi, A., Muñoz-Sabater, J., Nicolas, J., Peubey, C., Radu, R., Schepers, D., Simmons, A., Soci, C., Abdalla, S., Abellan, X., Balsamo, G., Bechtold, P., Biavati, G., Bidlot, J., Bonavita, M., De Chiara, G., Dahlgren, P., Dee, D., Diamantakis, M., Dragani, R., Flemming, J., Forbes, R., Fuentes, M., Geer, A., Haimberger, L., Healy, S., Hogan, R. J., Hólm, E., Janisková, M., Keeley, S., Laloyaux, P., Lopez, P., Lupu, C., Radnoti, G., de Rosnay, P., Rozum, I., Vamborg, F., Villaume, S., and Thépaut, J.-N.: The ERA5 global reanalysis, Q. J. Roy. Meteor. Soc., 146, 1999–2049, https://doi.org/10.1002/qj.3803, 2020.

Hobday, A. J., Alexander, L. V., Perkins, S. E., Smale, D. A., Straub, S. C., Oliver, E. C. J., Benthuysen, J. A., Burrows, M. T., Donat, M. G., Feng, M., Holbrook, N. J., Moore, P. J., Scannell, H. A., Sen Gupta, A., and Wernberg, T.: A hierarchical approach to defining marine heatwaves, Prog. Oceanogr., 141, 227–238, https://doi.org/10.1016/j.pocean.2015.12.014, 2016.

Hobday, A. J., Oliver, E. C. J., Sen Gupta, A., Benthuysen, J. A., Burrows, M. T., Donat, M. G., Holbrook, N. J., Moore, P. J., Thomsen, M. S., Wernberg, T., and Smale, D. A.: Categorizing and naming marine heatwaves, Oceanography, 31, 162–173, https://doi.org/10.5670/oceanog.2018.205, 2018.

Hochman, A., Scher, S., Quinting, J., Pinto, J. G., and Messori, G.: A new view of heat wave dynamics and predictability over the eastern Mediterranean, Earth Syst. Dynam., 12, 133–149, https://doi.org/10.5194/esd-12-133-2021, 2021.

IPCC: Climate Change 2021, The Physical Science Basis, Contribution of Working Group I to the Sixth Assessment Report of the Intergovernmental Panel on Climate Change, Cambridge University Press, https://doi.org/10.1017/9781009157896, 2021.

Jangir, B., Swain, D., and Ghose, S.: Influence of eddies and tropical cyclone heat potential on intensity changes of tropical cyclones in the North Indian Ocean, Adv. Space Res., 68, 773–786, https://doi.org/10.1016/j.asr.2020.01.011, 2021.

Jangir, B., Mishra, A. K., and Strobach, E.: Effects of mesoscale eddies on the intensity of cyclones in the Mediterranean Sea, J. Geophys. Res.-Atmos., 128, https://doi.org/10.1029/2023JD038607, 2023.

Jangir B., Mishra A. K., and Strobach, E.: The interplay between medicanes and the Mediterranean Sea in the presence of sea surface temperature anomalies, Atmos. Res., 310, 107625, https://doi.org/10.1016/j.atmosres.2024.107625, 2024.

Jangir, B., Reale, M., Menna, M., Mishra, A. K., Marellucci, R., Cossarini, G., Salone, S., Mauri, E., and Strobach, E.: The response of the physical and biogeochemical marine environment to the passage of Mediterranean cyclones in the presence of eddies, gyres, and marine heat wave, J. Geophys. Res.-Oceans, 131, https://doi.org/10.1029/2025JC023151, 2026.

Katsanos, D., Retalis, A., Kalogiros, J., Psiloglou, B. E., Roukounakis, N., and Anagnostou, M.: Performance Evaluation of Satellite Precipitation Products During Extreme Events – The Case of the Medicane Daniel in Thessaly, Greece, Remote Sens., 16, 4216, https://doi.org/10.3390/rs16224216, 2024.

Khodayar, S., Kushta, J., Catto, J. L., Dafis, S., Davolio, S., Ferrarin, C., Flaounas, E., Groenemeijer, P., Hatzaki, M., Hochman, A., Kotroni, V., Landa, J., Láng-Ritter, I., Lazoglou, G., Liberato, M. L. R., Miglietta, M. M., Papagiannaki, K., Patlakas, P., Stojanov, R., and Zittis, G.: Mediterranean cyclones in a changing climate: A review on their socio-economic impacts, Rev. Geophys., 63, https://doi.org/10.1029/2024RG000853, 2025.

Klein, P. and Lapeyre, G.: The Oceanic Vertical Pump Induced by Mesoscale and Submesoscale Turbulence, Annu. Rev. Mar. Sci., 1, 351–375, https://doi.org/10.1146/annurev.marine.010908.163704, 2009.

Kouroutzoglou, J., Flocas, H. A., Keay, K., Simmonds, I., and Hatzaki, M.: Climatological aspects of explosive cyclones in the Mediterranean, Int. J. Climatol., 31, 1785–1802, https://doi.org/10.1002/joc.2203, 2011.

Latha, P. T., Rao, K. H., Nagamani, P. V., Amminedu, E., Choudhury, S. B., Dutt, C. B. S., and Dadhwal, V. K.: Impact of Cyclone PHAILIN on Chlorophyll-a Concentration and Productivity in the Bay of Bengal, Int. J. Geosci., 6, 473–480, https://doi.org/10.4236/ijg.2015.65037, 2015.

Law, K.: The Impact of Oceanic Heat Content on the Rapid Intensification of Atlantic Hurricanes, Chap. 17, in: Recent Hurricane Research – Climate, Dynamics, and Societal Impacts, edited by: Lupo, A., Croatia, InTech, 331–354, https://doi.org/10.5772/13799, 2011.

Li, D., Chang, P., Ramachandran, S., Jing, Z., Zhang, Q., Kurian, J., Gopal, A., and Yang, H.: Contribution of the Two Types of Ekman Pumping Induced Eddy Heat Flux to the Total Vertical Eddy Heat Flux, Geophys. Res. Lett., 48, https://doi.org/10.1029/2021GL092982, 2021.

Lin, I. I., Goni, G. J., Knaff, J. A., Forbes, C., and Ali, M. M.: Ocean heat content for tropical cyclone intensity forecasting and its impact on storm surge, Nat. Hazards, 66, 1481–1500, https://doi.org/10.1007/s11069-012-0214-5, 2013.

Liu, Y., Tang, D., Tang, S., Morozov, E., Liang, W., and Sui, Y.: A case study of Chlorophyll a response to tropical cyclone Wind Pump considering Kuroshio invasion and air-sea heat exchange, Sci. Total Environ., 741, 140290, https://doi.org/10.1016/j.scitotenv.2020.140290, 2020.

MedECC: Climate and environmental change in the Mediterranean Basin – Current situation and risks for the future, in: First Mediterranean assessment report, edited by: Cramer, W., Guiot, J., and Marini, K., Union for the Mediterranean, Plan Bleu, UNEP/MAP, Marseille, France, 632 pp., ISBN: 978-2-9577416-0-1, 2020.

Menna, M., Martellucci, R., Reale, M. Cossarini, G., Salon, S., Notarstefano, G., Mauri, E., Poulain, P. M., Gallo, A., and Solidoro, C.: A case study of impacts of an extreme weather system on the Mediterranean Sea circulation features: Medicane Apollo (2021), Sci. Rep., 13, 3870, https://doi.org/10.1038/s41598-023-29942-w, 2023.

Miglietta, M. M. and Rotunno, R.: Development Mechanisms for Mediterranean Tropical-like Cyclones (Medicanes), Q. J. R. Meteorol. Soc., 145, 1444–1460, 2019.

Mishra, A. K., Jangir, B., and Strobach, E.: Influence of mesoscale sea-surface temperature structures on the Mediterranean cyclone Ianos in convection-permitting simulations: Contributions of surface warming and cold wakes, Q. J. R. Meteorol. Soc., 150, 5146–5166, https://doi.org/10.1002/qj.4862, 2024.

Morrow, R., Fu, L.-L., Ardhuin, F., Benkiran, M., Chapron, B., Cosme, E., d'Ovidio, F., Farrar, J. T., Gille, S. T., Lapeyre, G., Le Traon, P.-Y., Pascual, A., Ponte, A., Qiu, B., Rascle, N., Ubelmann, C., Wang, J., and Zaron, E. D.: Global Observations of Fine-Scale Ocean Surface Topography With the Surface Water and Ocean Topography (SWOT) Mission, Front. Mar. Sci., 6, 232, https://doi.org/10.3389/fmars.2019.00232, 2019.

Nicolaides, K. A., Michalelides, S. C., and Karacostas, T.: Synoptic and dynamic characteristics of selected deep depressions over Cyprus, Adv. Geosci., 7, 175–180, https://doi.org/10.5194/adgeo-7-175-2006, 2006.

Normand, J. C. L. and Heggy, E.: Assessing flash flood erosion following storm Daniel in Libya, Nat. Commun., 15, 6493, https://doi.org/10.1038/s41467-024-49699-8, 2024.

Oliver, E. C. J., Donat, M. G., Burrows, M. T., Moore, P. J., Smale, D. A., Alexander, L. V., Benthuysen, J. A., Feng, M., Sen Gupta, A., Hobday, A. J., Holbrook, N. J., Perkins-Kirkpatrick, S. E.,

Scannell, H. A., Straub, S. C., and Wernberg, T.: Longer and more frequent marine heatwaves over the past century, Nat. Commun., 9, 1324, https://doi.org/10.1038/s41467-018-03732-9, 2018.

Panegrossi, G., D'Adderio, L. P., Dafis, S., Rysman, J.-F., Casella, D., Dietrich, S., and Sanò, P.: Warm Core and Deep Convection in Medicanes, A Passive Microwave-Based Investigation, Remote Sens., 15, 2838, https://doi.org/10.3390/rs15112838, 2023.

Pytharoulis, I., Kartsios, S., Tegoulias, I., Feidas, H., Miglietta, M. M., Matsangouras, I., and Karacostas, T.: Sensitivity of a Mediterranean Tropical-Like Cyclone to Physical Parameterizations, Atmosphere, 9, 436, https://doi.org/10.3390/atmos9110436, 2018.

Rathore, S., Goyal, R., Jangir, B., Ummenhofer, C. C., Feng, M., and Mishra, M.: Interactions Between a Marine Heatwave and Tropical Cyclone Amphan in the Bay of Bengal in 2020, Front. Clim., 4, 861477, https://doi.org/10.3389/fclim.2022.861477, 2022.

Raveh-Rubin, S. and Flaounas, E.: A dynamical link between deep Atlantic extratropical cyclones and intense Mediterranean cyclones, Atmos. Sci. Lett., 18, 215–221, https://doi.org/10.1002/asl.745, 2017.

Reale, M., Cabos Narvaez, W. D., Cavicchia, L., Conte, D., Coppola, E., Flaounas, E., Giorgi, F., Gualdi, S., Hochman, A., Li, L., Lionello, P., Podrascanin, Z., Salon, S., Sanchez-Gomez, E., Scoccimarro, E., Sein, D. V., and Somot, S.: Future projections of Mediterranean cyclone characteristics using the Med-CORDEX ensemble of coupled regional climate system models, Clim. Dyn., 58, 2501–2524, https://doi.org/10.1007/s00382-021-06018-x, 2022.

Reynolds, R. W., Smith, T. M., Liu, C., Chelton, D. B., Casey, K. S., and Schlax, M. G.: Daily High-Resolution-Blended Analyses for Sea Surface Temperature, J. Climate, 20, 5473–5496, https://doi.org/10.1175/2007JCLI1824.1, 2007.

Scardino, G., Miglietta, M. M., Kushabaha, A., Casella, E., Rovere, A., Besio, G., Borzì, A. M., Cannata, A., Mazza, G., Sabato, G., and Scicchitano, G.: Fingerprinting Mediterranean hurricanes using pre-event thermal drops in seawater temperature, Sci. Rep., 14, 8014, https://doi.org/10.1038/s41598-024-58335-w, 2024.

Scardino, G., Kushabaha, A., Miglietta, M. M., Bonaldo, D., and Scicchitano, G.: When storms stir the Mediterranean depths: chlorophyll *a* response to Mediterranean cyclones, Ocean Sci., 21, 2849–2872, https://doi.org/10.5194/os-21-2849-2025, 2025.

Shang, X.-D., Zhu, H.-B., Chen, G.-Y., Xu, C., and Yang, Q.: Research on cold core eddy change and phytoplankton bloom induced by typhoons, Case studies in the South China Sea, Adv. Meteorol., 1–19, https://doi.org/10.1155/2015/340432, 2015.

Sharma, V. and Ali, M. M.: Importance of ocean heat content for cyclone studies, Journal of Oceanography and Marine Research, 2, 1–6, https://www.longdom.org/open-access (last access: 13 May 2026), 2014.

Stern, M.: Interaction of a uniform wind stress with a geostrophic vortex, Deep-Sea Res. Oceanogr. Abstr., 12, 355–367, 1965.

Strobach, E., Mishra, A. K., Jangir, B., Ziv, B., Sun, R., Siegelman, L., Meroni A. N., and Klein, P.: Intensification of a rain system imparted by Mediterranean mesoscale eddies, Sci. Rep., 14, 26810, https://doi.org/10.1038/s41598-024-76767-2, 2024.

Sun, M., Tian, F., Liu, Y., and Chen, G.: An Improved Automatic Algorithm for Global Eddy Tracking Using Satellite Altimeter Data, Remote Sens., 9, 206, https://doi.org/10.3390/rs9030206, 2017.

Teruzzi, A., Di Biagio, V., Feudale, L., Bolzon, G., Lazzari, P., Salon, S., Coidessa, G., and Cossarini, G.: Mediterranean Sea Biogeochemical Reanalysis (CMEMS MEDBiogeochemistry, MedBFM3 system), Version 1, Copernicus Monitoring Environment Marine Service (CMEMS) [data set], https://doi.org/10.25423/CMCC/MEDSEA_MULTIYEAR_BGC_006_008_MEDBFM3, 2021a.

Teruzzi, A., Feudale, L., Bolzon, G., Lazzari, P., Salon, S., Di Biagio, V., Coidessa, G., and Cossarini, G.: Mediterranean Sea Biogeochemical Reanalysis INTERIM (CMEMS MED-Biogeochemistry, MedBFM3i system), Version 1, Copernicus Monitoring Environment Marine Service (CMEMS) [data set], https://doi.org/10.25423/CMCC/MEDSEA_MULTIYEAR_BGC_006_008_MEDBFM3I, 2021b.

Tranchant, Y. T., Legresy, B., Foppert, A., Pena-Molino, B., and Phillips, H.: SWOT reveals fine-scale balanced motions and dispersion properties in the Antarctic Circumpolar Current, ESS Open Archive [preprint], https://doi.org/10.22541/essoar.173655552.25945463/v1, 2025.

Trigo, I. F., Bigg, G. R., and Davies, T. D.: Climatology of cyclogenesis mechanisms in the Mediterranean, Mon. Weather Rev., 130, 549–569, 2002.

Vidya, P. J., Balaji, M., and Mani Murali, R.: Cyclone Hudhud-eddy induced phytoplankton bloom in the northern Bay of Bengal using a coupled model, Prog. Oceanogr., 197, 102631, https://doi.org/10.1016/j.pocean.2021.102631, 2021.

Volpe, G., Buongiorno Nardelli, B., Colella, S., Pisano, A., and Santoleri, R.: An Operational Interpolated Ocean Colour Product in the Mediterranean Sea, in: New Frontiers in Operational Oceanography, edited by: Chassignet, E. P., Pascual, A., Tintorè, J., and Verron, J., 227–244, https://doi.org/10.17125/gov2018.ch09, 2018.

Volpe, G., Colella, S., Brando, V. E., Forneris, V., La Padula, F., Di Cicco, A., Sammartino, M., Bracaglia, M., Artuso, F., and Santoleri, R.: Mediterranean ocean colour Level 3 operational multi-sensor processing, Ocean Sci., 15, 127–146, https://doi.org/10.5194/os-15-127-2019, 2019.

Wada, A. and Usui, N.: Importance of tropical cyclone heat potential for tropical cyclone intensity and intensification in the Western North Pacific, J. Oceanogr., 63, 427–447, https://doi.org/10.1007/s10872-007-0039-0, 2007.

Zhang, Z. and Qiu, B.: Surface Chlorophyll Enhancement in Mesoscale Eddies by Submesoscale Spiral Bands, Geophys. Res. Lett., 47, https://doi.org/10.1029/2020GL088820, 2020.

Zhao, Z. and Marin, M.: A MATLAB toolbox to detect and analyze marine heatwaves, Journal of Open Source Software, 4, 1124, https://doi.org/10.21105/joss.01124, 2019.

Zittis, G., Almazroui, M., Alpert, P., Ciais, P., Cramer, W., Dahdal, Y., Fnais, M., Francis, D., Hadjinicolaou, P., Howari, F., Jrrar, A., Kaskaoutis, D. G., Kulmala, M., Lazoglou, G., Mihalopoulos, N., Lin, X., Rudich, Y., Sciare, J., Stenchikov, G., Xoplaki, E., and Lelieveld, J.: Climate change and weather extremes in the Eastern Mediterranean and Middle East, Rev. Geophys., 60, https://doi.org/10.1029/2021RG000762, 2022.